HHS Public Access

Author manuscript

*Am J Ophthalmol*. Author manuscript; available in PMC 2015 September 01.

Published in final edited form as:

*Am J Ophthalmol*. 2014 September ; 158(3): 584–96.e1. doi:10.1016/j.ajo.2014.05.038.

# Photoreceptor perturbation around subretinal drusenoid deposits revealed by adaptive optics scanning laser ophthalmoscopy

**Yuhua Zhang**[1,*], **Xiaolin Wang**[1], **Ernesto Blanco Rivero**[1], **Mark E Clark**[1], **Clark Douglas Witherspoon**[1], **Richard F Spaide**[2], **Christopher A. Girkin**[1], **Cynthia Owsley**[1], and **Christine A. Curcio**[1]

[1]Department of Ophthalmology, University of Alabama at Birmingham School of Medicine, Birmingham, Alabama

[2]Vitreous-Retina-Macula Consultants of New York, New York

## Abstract

**Purpose—**To describe the microscopic structure of photoreceptors impacted by subretinal drusenoid deposits, also called pseudodrusen, an extracellular lesion associated with age-related macular degeneration (AMD), using adaptive optics scanning laser ophthalmoscopy (AOSLO).

**Design—**Observational case series.

**Methods—**Fifty-three patients with AMD and 10 age-similar subjects in normal retinal health were recruited. All subjects underwent color fundus photography, infrared reflectance, red-free reflectance, autofluorescence, and spectral-domain optical coherence tomography (SD-OCT). Subretinal drusenoid deposits were classified with a 3-stage OCT-based grading system. Lesions and surrounding photoreceptors were examined with AOSLO.

**Results—**Subretinal drusenoid deposits were found in 26 eyes of 13 patients with AMD and imaged by AOSLO and SD-OCT in 18 eyes (n=342 lesions). SD-OCT showed subretinal drusenoid deposits as highly reflective material accumulated internal to the retinal pigment epithelium. AOSLO revealed that photoreceptor reflectivity was qualitatively reduced by stage 1 subretinal drusenoid deposits and greatly reduced by stage 2. AOSLO presented a distinct structure in stage 3, a hyporeflective annulus consisting of deflected, degenerated or absent photoreceptors. A central core with a reflectivity superficially resembling photoreceptors is formed by the lesion material itself. A hyporeflective gap in the photoreceptor ellipsoid zone on



[*]Inquiries to Yuhua Zhang, PhD, Department of Ophthalmology, University of Alabama at Birmingham School of Medicine, Volker Hall 390C, 1670 University Boulevard, Birmingham, AL 35294. Phone: 205-996-8663, Fax: 205-934-3425, zhanghua@uab.edu.

**DISCLOSURE:**

ALL AUTHORS HAVE COMPLETED AND SUBMITTED THE ICMJE FORM FOR DISCLOSURE OF POTENTIAL CONFLICTS OF INTEREST. Zhang, Wang, Blanco, Clark, Witherspoon, Girkin, Owsley, and Curcio reported no potential interest.

either side of this core shown in SD-OCT corresponded to the hyporeflective annulus seen by AOSLO.

**Conclusions—**AOSLO and multimodal imaging of subretinal drusenoid deposits indicate solid, space filling lesions in the subretinal space. Associated retinal reflectivity changes are related to lesion stages and are consistent with perturbations to photoreceptors, as suggested by histology.

## INTRODUCTION

Pseudodrusen were first described by Mimoun et al as a distinctive yellowish pattern that was “visible en lumière bleue” (visible in blue light) in some eyes with age-related macular degeneration (AMD).[1] Because the lesions appeared different from typical drusen and were angiographically silent, the authors thought they were deep to the retinal pigment epithelium (RPE). Arnold and Sarks found that pseudodrusen were more easily visualized with red-free (RF) light or with a He-Ne laser scanning laser ophthalmoscope (SLO).[2] On the basis of one histological specimen lacking neurosensory retina, they proposed that pseudodrusen appearance arose from choroidal fibrosis. Lois et al described a reticular pattern of autofluorescence in eyes with AMD.[3] Smith et al reported that 87.5% of eyes with a reticular autofluorescence pattern also had pseudodrusen corresponding in part with the autofluorescence,[4] later speculating that both phenomena were manifestations of a reticular macular disease involving the RPE, choriocapillaris, and inner choroidal.[5] With spectral domain optical coherence tomography (SD-OCT), Zweifel et al found that pseudodrusen correlated to granular hyper-reflective materials deposited anterior to the RPE in the subretinal space;[6] other than generalized choroidal thinning, no specific choroidal abnormality was seen. By comparing OCT findings to histologic examination of 1 donor retina with extracellular material between the RPE and photoreceptors called subretinal drusenoid deposits,[7] Zweifel et al attributed pseudodrusen appearance to these lesions. Subsequent SLO and OCT imaging studies reached the same conclusion.[8, 9] However, Sohrab et al stated that subretinal deposits and photoreceptor disturbances on OCT did not co-localize with pseudodrusen and speculated how pseudodrusen appearance could arise secondarily from choroidal fibrosis.[10] Suzuki et al recently defined 3 subtypes of clinical pseudodrusen, all corresponding to a subretinal reflectivity visible by OCT.[11] Thus the location of pseudodrusen within the chorioretinal layers has been a subject of debate, with evidence for the subretinal space accumulating.

In clinicopathologic studies, Sarks et al showed that membranous debris, the principal component of soft drusen and basal linear deposit, was also found in the subretinal space.[12] Curcio and co-workers demonstrated that these subretinal materials shared partial molecular commonality with drusen, including unesterified cholesterol, apolipoprotein E, complement factor H, and vitronectin. Esterified cholesterol, however, was undetectable, as was immunoreactivity for photoreceptor, Müller cell, and RPE marker proteins.[7, 13] Subretinal drusenoid deposits were proposed as the correlate to pseudodrusen by these authors, because the size, distribution, and prevalence of the material seen in a series of 22 donor eyes corresponded so closely to pseudodrusen imaged clinically by several methods.[14] In one case reported by the Sarks and coworkers, an eye with pseudodrusen was examined histologically and found to correlate with subretinal material.[15] These authors declined to

attribute all pseudodrusen to such deposits, however, because the smallest ones were not detectable clinically.

Given the paucity of histologic examination of clinically characterized eyes, two recent advances in ocular imaging have made it possible to address questions of pseudodrusen localization *in vivo*. First, the living retina can be imaged with significantly improved resolution and precision in three dimensions. SD-OCT can image cross-sections of retina and choroid with sufficient resolution to reveal cellular and subcellular stratifications.[16, 17] A recent study has demonstrated the feasibility of using adaptive optics (AO) to image cones in the maculae of patients with pseudodrusen.[18] However, the study was conducted with a flood-illuminated AO imaging system that does not possess depth discrimination capability. AO assisted confocal SLO (AOSLO)[19–24] has improved depth discrimination ability to form images from light emanating from the selected plane in the fundus. Multimodal imaging featuring AOSLO thus has the potential to answer whether the histological correlates of pseudodrusen are in the subretinal space. Secondly, information from multiple imaging technologies can be readily merged to bring the advantages of each individual technique to bear on a single question, resulting in a more comprehensive understanding. Therefore, the purpose of the present study was 2-fold: to correlate AOSLO findings with SD-OCT to precisely determine the laminar localization of pseudodrusen and to investigate how the AOSLO findings inform the imaging characteristics of pseudodrusen obtained by other more established modalities.

## METHODS

The study followed the tenets of the Declaration of Helsinki and was approved by the Institutional Review Board at the University of Alabama at Birmingham. Written informed consent was obtained from participants after the nature and possible consequences of the study were explained. The study complied with the Health Insurance Portability and Accountability Act of 1996.

- **Nomenclature:** In previous studies, the terms reticular pseudodrusen, pseudo-reticular drusen, or pseudodrusen was used for different *en face* modalities[2, 8, 15, 25–32], and the term subretinal drusenoid deposits for cross-sectional histology and SD-OCT[6, 7, 32, 33] In the present article, we will use the term pseudodrusen for standard *en face* ophthalmoscopy (color fundus photography, infrared reflectance (IR), red-free (RF), and autofluorescence (AF)) and the term subretinal drusenoid deposits for the collections of material seen in the subretinal space in histologic specimens, AOSLO, and OCT.
- **Patients and controls:** Study patients with AMD and age-similar subjects with normal retinas were recruited from the clinical research registry of the Department of Ophthalmology of the University of Alabama at Birmingham and through the Retina Service. The patients have been diagnosed with AMD previously. To assess the disease severity, stereoscopic color digital 30° fundus photographs were taken with a FF450 Plus fundus camera (Carl Zeiss Meditec, Dublin, CA) after pupil dilation, and photographs were graded by a masked, experienced grader using the Age-Related Eye Disease Study 2 (AREDS2) severity scale for AMD.[34] Disease

severity ranged from early to advanced (AREDS grade 2–11). Participants in normal macular health met the criteria for AREDS grade 1 in both eyes. Exclusion criteria included diabetes, history of retinal vascular occlusions, and any signs or history of hereditary retinal dystrophy. Subjects were also excluded for reasons that might potentially prevent successful imaging, such as poor fixation, significant media opacity, irregular pupil shape, poor dilation, or refractive errors beyond ±6 D spherical and ±3 D cylinder. The inclusion criteria for normal comparison subjects were the same, with the additional criteria of age greater than 50 years, no clinically significant cataract, and best-corrected visual acuity (BCVA) of 20/25 or better.

- **High-resolution AOSLO imaging:** Imaging was conducted with a new generation AOSLO that was developed in our lab, as described.[35, 36] This instrument was based upon an earlier prototype that used a micro-electric-mechanic-system based deformable mirror.[20] The new instrument addressed several major obstacles that impede imaging of older patients with AMD. First, the pupil size decreases and wavefront aberration increases with aging. Second, many older patients have cataract, which significantly affects wavefront detection and impairs AO wavefront correction. Third, in patients with intraocular lenses, it is very common that proliferation and transformation of lens epithelial cell remnants lead to posterior capsular opacification or fibrosis over the intraocular lens. While capsulotomy can make an opening on the opacified posterior capsule, the clear pupil for imaging often has an irregular shape. This may not only reduce the useful pupil size but also cause complicated light scattering that impedes AO operation.

  To address these challenges, we developed advanced wavefront detection and correction strategy. We designed a high-speed Shack-Hartmann wavefront sensor based upon a complementary metal–oxide–semiconductor (CMOS) camera (MicroVista®-NIR, Intevac Inc. CA). The camera's spectral response is optimized for the imaging light used by AOSLO, enabling the AO system to be operated at a loop frequency up to 100 Hz. Most previously reported AO systems for retinal imaging run under 30 Hz. High-speed wavefront sensing significantly facilitates advanced control strategy based upon Zernike mode correction, thereby allowing for AO correction of wavefronts in eyes with the optical problems described above. Furthermore, we adopted a high-speed deformable mirror (Hi-Speed DM97-15, ALPAO SAS, France) with 97 actuators with stroke up to 30 which provides improved ability[37] to compensate for increased high orders and amplitude of wavefront aberration due to aging.[38] The AOSLO pupil size was set at 5.6 mm in diameter. After AO correction, the root-mean-square wave aberration was reduced to less than 0.05 μm in most eyes, reaching the criterion for diffraction-limited resolution for the light used in imaging. A low coherence light source, a superluminescent diode (Broadlighter S840-HP, Superlum, Russia), was employed for producing high fidelity retinal images.[39] The imaging light power measured at the cornea was 500 μWatts, which is about 1/26 of the maximum permitted exposure limits set by the ANSI standard.[40] The AOSLO records continuous videos from the eye with a frame rate 15 Hz.

All participants underwent BCVA measurement by the Electronic Visual Acuity (EVA) protocol.[41] Pupils were dilated with 1.0% tropicamide and 2.5% phenylephrine hydrochloride. The subject's head was aligned and stabilized using a head-mount with a chin-rest. A fixation target consisting of a moving bright green light dot formed by the light from a laser diode (DJ532-10- 532, Thorlabs Inc, Newton, NJ) on a calibrated grid. The grid, on white paper, was placed in front of the eye via a pellicle beam splitter (BP208, Thorlabs Inc, Newton, NJ) to help the subject's fixation. The wavelength of the diode laser is 532 nm and the light was coupled into a single mode fiber and collimated to form a light dot of 1.5 mm diameter on the grid paper. The light power was adjusted to 2 mW at the output of the fiber. The subject saw the light dot on the back of the grid paper through the pellicle beam splitter. During imaging, the dot was moved on the grid paper to direct the subject's view angle. At each grid point, the light dot stopped for 3–5 seconds so that 45–75 frames were acquired. Videos were recorded continuously across an area of 15 X 15°. An AOSLO imaging session lasted approximately 1 hour. Data presented were collected from one imaging session for each subject. Before images were recorded, the gain of the AOSLO photo-detector was titrated to obtain proper image brightness and contrast according to a real-time histogram of a retinal video and remained constant through the whole imaging session.

- **AOSLO image processing, and analysis:** Image distortions caused by nonlinearities in the resonant scanner and by eye movements were eliminated by customized software.[42] Registered images were averaged to enhance signal-to-noise ratio. Images of different retinal locations were manually aligned on a cell-to-cell basis to create a continuous montage (Photoshop, Adobe Systems Inc., Mountain View, CA).

  AOSLO image pixel size was computed from an image of a precisely calibrated dot grid placed at the retinal plane of a model eye. The extent of retina affected by the underlying subretinal drusenoid deposits at different progression stages was measured at multiple locations using the Ruler Tool of Photoshop and then averaged.

- **Multimodal imaging:** In addition to stereoscopic color digital 30° fundus photographs, *en face* IR (λ = 830 nm), RF (λ = 560 nm), and AF (excitation, 488 nm; emission, > 600 nm) images were acquired with the confocal SLO of the Spectralis (Heidelberg Engineering, Carlsbad, CA). Fields of view of 30° × 30° were digitized at 768 × 768 pixels. Retinal cross-sections were imaged with the Spectralis SD-OCT (λ = 870 nm; acquisition speed, 40,000 A-scans per seconds; scan depth, 1.9 mm; digital depth resolution, 3.5 μm per pixel in tissue; lateral resolution in tissue 14 μm). In each study eye, 97 B-scans were acquired across a 15° × 10° area of the central macula to create a volume.

- **Pseudodrusen identification:** Multiple imaging modalities can disclose pseudodrusen, with different specificity and sensitivity.[30] It is recommended that detection should be confirmed using more than one modality for improving accuracy.[30, 31] The identification of pseudodrusen in our study was based on their

presence in at least 2 *en face* imaging modalities and in SD-OCT.[27, 29, 32] In *en face* imaging, pseudodrusen appear as an interlacing collection of ribbons or a dot-like pattern of yellow-white lesions (in color fundus photography), a pattern of hypo-reflective or hyper-reflective spots (in IR reflectance), or a pattern of small hypo-autofluorescent areas against a background of mild hyper-autofluorescence (in AF). Although a reticular pattern was often seen in color photography, it was not a criterion for diagnosis. In SD-OCT, subretinal drusenoid deposits were hyper-reflective mounds internal to the RPE. Axial microstructure and location of subretinal drusenoid deposits were evaluated with SD-OCT, using the nomenclature of Spaide and Curcio for the 4 outer retinal hyper-reflective bands.[43–45]

- **Multimodal image registration:** Color fundus photographs and IR, RF, AF images taken with the Spectralis SLO were registered manually by use of retinal vessels and capillaries as invariant landmarks. Color fundus photographs and the SLO IR image were then magnified and registered with the AOSLO montage by use of retinal vessels and capillaries as landmarks. Then pseudodrusen apparent on standard funduscopy were localized in AOSLO images and examined with high resolution.
- **Subretinal drusenoid deposits classification:** Lesions were scored with the 3-stage grading system introduced by Zweifel et al.[6] Specific lesions at each stage and surrounding photoreceptors were examined by AOSLO and by *en face* OCT.

## RESULTS

A total of 63 subjects (33 males and 30 females) were enrolled from October 2010 to January 2013, including 53 AMD patients (73.50 ± 8.08 years, mean ± SD) and 10 control subjects (64.0 ± 9.93 years). All subjects were white and non-Hispanic. Subretinal drusenoid deposits were found in 26 eyes of 13 AMD patients (13/53: 24.5%). One eye (1/26: 4%) was at AREDS grade 4 (early stage); 16 eyes (16/26: 62%) were at AREDS grade 5–8 (intermediate stage); 4 eyes (4/26: 15%) were at AREDS grade 9–10 (advanced stage, GA); 5 eyes (5/26: 19%) were at AREDS grade 11 (advanced stage, CNV). Eleven patients had both subretinal drusenoid deposits and conventional sub-RPE drusen, and 2 patients had only subretinal drusenoid deposits. AOSLO imaged 18 eyes from 11 patients. Two (4 eyes) patients were not imaged by AOSLO due to small pupil (subject 2, AREDS OD:5, OS:5) and poor fixation (subject 7, AREDS OD:11, CNV, OS:9, GA). No subretinal drusenoid deposits were found in eyes at AREDS grade 1.

Figure 1 shows images of a normal subject. AOSLO revealed clearly the mosaic of cone and rod inner segments across the macula. While individual photoreceptors manifested varying brightness,[46, 47] brightness is similar across clusters of adjacent photoreceptors; accordingly, SD-OCT revealed even and well-aligned outer retinal hyper-reflective bands without discernible hyper-reflective material between RPE and EZ bands.

The effects of subretinal drusenoid deposits on surrounding cells were readily imaged with AOSLO at different lesion stages. At stage 1 (Figure 2), the EZ band undulates due to a

granular hyper-reflective material accumulated between it and the RPE band. The overlying photoreceptors exhibit reduced reflectivity, and the mosaic is undetectable by AOSLO. At stage 2 (Figure 3), the EZ band was appreciably deflected inwardly by mounds of accumulated material. The retina superjacent to each lesion shows further reduced overall reflectance, and individual photoreceptors are no longer visible by AOSLO. At stage 3 (Figure 4), subretinal drusenoid deposits have interrupted the EZ band and extended to the inwardly deviated ELM. Surrounding the lesion apex is a region of absent OCT signal from the EZ and a lack of visualized cones. By AOSLO, the retina immediately adjacent to subretinal drusenoid deposits shows a hyporeflective annular zone with indistinct photoreceptors, which corresponds to the hyporeflective EZ gaps. As discussed in the next section, this annular zone may contain missing, degenerated, or deflected photoreceptors. AOSLO also reveals within the annulus a reflective center area with a granular structure that is similar to the surrounding retina (bottom left panel of Figure 4, and top panel of Figure 5). Outside the annulus the cone mosaic resumes, albeit at variable reflectivity levels relative to normal photoreceptors (Figure 1). *En face* OCT imaging (Figure 5, bottom row) of a large solitary subretinal drusenoid deposit also shows a hyporeflective annulus of the stage 3 lesion like that revealed by AOSLO. The hyper-reflective center in AOSLO imaging is the subretinal drusenoid deposit material itself, as confirmed by en-face reconstruction of OCT scans (Figure 5, bottom row), as well as AO assisted SD-OCT.[36]

We assessed by AOSLO 342 subretinal drusenoid deposits that could also be identified on SD-OCT scans and all localized to the subretinal space. Of these, 63 could be classified as stage 1, 118 stage 2, and 171 stage 3. Subretinal drusenoid deposits associated impact on photoreceptors by stages is shown in the Table, which lists the diameters of the quasi-circular areas of overlying retina affected by individual deposits. The inner diameters of stage 3 subretinal drusenoid deposits' reflective cores are the diameters of lesions themselves.

## DISCUSSION

Using AOSLO, we observed that defined stages of subretinal drusenoid deposits were associated with reflectivity changes consistent with perturbed surrounding photoreceptors. AOSLO revealed a distinct *en face* structure of stage 3 subretinal drusenoid deposits (Figures 4–5) with a hyporeflective annular zone containing indistinct photoreceptors and surrounding a reflective central area. AOSLO imaging in conjunction with SD-OCT suggested that the hyporeflective annulus likely consists of photoreceptors with deflected, degenerated, or missing inner or outer segments, and the reflective core of stage 3 lesions is the subretinal drusenoid deposits material itself.

Our results are informed by the imaging mechanism of AOSLO, which draws on principles of confocal microscopy [48] and waveguide properties of photoreceptors.[49, 50] The photoreceptors of the living human eye have waveguiding properties, as evidenced by the Stiles–Crawford effect observed for light incident near the pupil rim,[51] and by the directional component of light reflected off the retina in the related optical Stiles–Crawford effect (OSCE).[52, 53] In a normal eye the photoreceptors are oriented with their central axis toward a point near the pupil center. This is the configuration that allows the photoreceptors

to couple the incident light with the highest efficiency. AOSLO is essentially a confocal microscope that uses the human eye as its objective lens. To produce a clear photoreceptor mosaic, AOSLO imaging light is focused at the anterior aspect of the inner segments,[39] near the ELM. This is the anatomic axial position where light enters and emerges from the fiber-optic portion of the photoreceptor.[54] AOSLO has an axial resolution of 50–70 μm with the AO correction for ocular optical wave aberration,[20, 23] implying that AOSLO images are formed by the aggregate light reflected from an axial (3D) volume (3 μm x 3 μm x 50 μm with our AOSLO) from the ELM to the apical surface of the RPE (Figure 5, middle-right panel, levels 1–4), i.e., the portion of the inner and outer segments of the photoreceptors. Structures outside of this volume are not imaged.[48] In a normal eye, the OSCE produces a peaked intensity distribution of directional light returned from the photoreceptor toward the pupil center.[55–57] The directional light returned from the photoreceptor is caught by the AOSLO thus normal orientation of the photoreceptors plays an important role in forming a clear image of them. In other words, only those photoreceptors maintain normal alignment can be imaged by the AOSLO. In a healthy retina, photoreceptors pack tightly in a matrix with their normal orientation toward to the pupil center thus the AOSLO renders a clear mosaic of the photoreceptor inner segments across the retina (Figure 1). A large dark area, such as the hyporeflective annulus revealed around the stage 3 subretinal drusenoid deposit, with indistinct photoreceptors in an AOSLO image may thus imply that photoreceptors are with misaligned, or degenerate, or even missing inner or outer segments. A deflected photoreceptor is neither able to funnel incident light into inner and outer segments nor reflect light back towards the AOSLO detector, thus leading to undetectability. Similarly, for a photoreceptor with a degenerating or missing outer segment and a subsequently degenerating inner segment, light for imaging will be reduced or absent. This point can be explained by a model attributing AOSLO images of photoreceptors to light reflected mostly from the EZ and outer segment tips.[39] Recently, Meadway et al used directional OCT, a technique proposed by Lujan et al,[58] to preliminarily confirm that the hyporeflective annulus surrounding stage 3 subretinal drusenoid deposits contains deflected photoreceptors (Meadway A, et al. IOVS 2014;55:ARVO E-Abstract 1592).

One interesting question is why the EZ appears intact over stage 1 and 2 lesions in OCT, when reflectivity revealed by AOSLO over these lesions is clearly reduced. Several phenomena may contribute to this finding. The OCT instrument used in this study has a lateral resolution of 14 μm. The diameter of the lateral point spread function of the OCT (diameter of the light focus waist) is 28 μm, which covers approximately 25 times more photoreceptors than the AOSLO light focus (diameter of 5.6 μm). Thus, as long as some cones appear, OCT will show a bright pixel, formed by light from a thick slab of the retina, and EZ bands over stage 1 and 2 subretinal drusenoid deposits will appear visible and continuous. Further, OCT forms images with a coherent detection mechanism that uses a reference beam that multiplies the signal from the reflections. B-scans presented in figures have been averaged for 36 frames, significantly improving the signal to noise ratio. Finally and very importantly, the OCT images are rendered in logarithmic grey scale. All these factors contribute to photoreceptors being more visible in the EZ band (imaged by OCT) than they are by AOSLO.

Our study can be compared to and differentiated from the recent report of markedly decreased reflectivity attributable to photoreceptors over subretinal drusenoid deposits by Mrejen et al, who used a commercial flood illumination AO fundus camera.[18] We imaged a larger sample of lesions (342 vs 55 subretinal drusenoid deposits) in more eyes (18 vs 11) and assessed reflectivity changes with respect to an SD-OCT based grading scale for these lesions. Our study suggests that the reflective spots over subretinal drusenoid deposits reported by these authors may have included non-photoreceptor reflectivity that can be attributed to the lesion itself as well as photoreceptors. Compared to the instrument used by Mrejen et al, our AOSLO system has confocal imaging, more actuators on the deformable mirror, a high speed wavefront sensor, and a low coherent light source with broader spectrum (center wavelength 840 nm, bandwidth 60 nm) to further reduce interference artifacts.[35, 36, 39] With these technical advantages we observed that the packing density of granules in the centers of stage 3 subretinal drusenoid deposit was similar to or higher than that of presumably healthy photoreceptors outside the dark annulus (Fig. 4 and Fig. 5).[36] This finding would be considered counter-intuitive, if the particulate reflectivity represents only cone photoreceptors, because histology suggests impaired cone survival over stage 3 subretinal drusenoid deposits.[7, 14] However, for a large proportion of stage 3 lesions seen by SD-OCT, the lesion apex bumped up against the ELM or poked through it (Figures 4 and 5). Therefore, any *en face* image that showed inner segments of surrounding cones also had to contain a reflective core attributable to the lesion itself. In a separate report, we confirmed this interpretation using AOSLO and AO assisted SD-OCT to view single subretinal drusenoid deposits in both *en face* and cross-sectional planes.[36] The AO SD-OCT clearly revealed a pile of hyper-reflective granules. AOSLO imaging at different focal planes showed that the central granules, while manifesting variable reflectivity with the change of light focus, retained a fairly stable packing structure. This strongly suggests that the speckled texture in both modes arises from the granular nature of the lesions. However, the flood illumination AO fundus camera was unable to reveal these structures to the extent presented by AOSLO. Thus, if counts of cones over subretinal drusenoid deposits assessed by Mrejen et al were included non-photoreceptor reflectivity in this manner,[18] then the severe photoreceptor degeneration associated with stage 3 subretinal drusenoid deposits reported by those authors may actually be worse.

Our study supports the hypothesis that pseudodrusen appearance is attributable to subretinal drusenoid deposits. Given the AOSLO focusing plane in the retina, the axial resolution, and clear photoreceptor mosaic in retina surrounding subretinal drusenoid deposits, reduced photoreceptor reflectivity associated with stage 1 and 2 subretinal drusenoid deposits represents alterations in the subretinal space. For stage 3 subretinal drusenoid deposits, photoreceptors and space-occupying materials clearly imaged by OCT are also in the same focal plane. Our most definitive evidence is that all 342 pseudodrusen identified in registered AOSLO, color, IR, RF, and AF images were examined in SD-OCT volume scans and found in the subretinal space. Further, a pseudodrusen subtype that extends into peripheral retina beyond the range of our AOSLO imaging in this study also localizes exclusively to the subretinal space.[11] On the basis of these two datasets, pseudodrusen and subretinal drusenoid deposits appear to be one and the same, although any individual lesion in any individual eye may be better visualized with one imaging modality or another. Any

pseudodrusen in the macula that are not also subretinal drusenoid deposits may thus be rare to non-existent. As the name pseudodrusen implies something false, we recommend the subretinal drusenoid deposits terminology for these lesions, as visualized in all modalities.

This study has identified areas requiring future research. Subretinal drusenoid deposits have been classified into multiple subtypes, of which we measured the size of solitary lesions only, recently termed dots.[11] Our classification system remains subjective, and we measured the size of subretinal drusenoid deposits manually. Confirmation of photoreceptor perturbation via functional assays like microperimetry would be ideal. Although a physical object in the subretinal space well explains pseudodrusen appearance, formation of these lesions is multifactorial. Additional insights into subretinal drusenoid deposits biogenesis will require detailed imaging studies directed toward factors that we did not herein address due to limitations of current AOSLO technology. These include RPE status (via fundus autofluorescence) and choroidal physiology (via enhanced depth imaging, phase sensitive OCT, or OCT with longer wavelength imaging light). The latter is important given current interest in the complex role of choroidal thickness.[59–62] In a histologic study of 22 eyes of 20 donors with early AMD choriocapillary ghosts were seen in 12.7% of regions under subretinal drusenoid deposits as compared with 7.7% lacking lesions; [14] such relative preservation was not visualized in vivo.[10, 63]

In conclusion, our study presents an improved description with multimodal high resolution imaging of a major component of AMD pathology localizing to the subretinal space. If extended with longitudinal data in more patients, these results would deepen our mechanistic understanding of AMD and how it is studied. Subretinal drusenoid deposits are inadequately represented in the AMD grading systems that provide the basis of population prevalence estimates and genetic associations, including a recent system that developed contemporaneously with high-resolution imaging studies hinting at the magnitude of these lesions.[64] Proper functioning of photoreceptors depends on a bi-directional transport of molecules between them and the RPE that could be inhibited by material occupying space in the subretinal space. Extracellular material in the subretinal space lacks intrinsic cellular anti-oxidant systems, perhaps rendering this material susceptible to oxidative damage with pro-angiogenic outcomes. Our data strengthen the reality of subretinal drusenoid deposits and help motivate new studies to understand their significance.

## Acknowledgments

Spaide RF receives consultant and royalty payment support from Topcon Inc, Tokyo, Japan, and receives consultant payment support from Bausch and Lomb, Rochester, New York, USA. This project was supported in part by EyeSight Foundation of Alabama (YZ), International Retina Research Foundation (YZ), 5R21EY021903 (YZ), Songs for Sight (CAG), Buck Trust of Alabama (CAG), R01AG04212 (CO), and R01EY06109 (CC) and institutional support from Research to Prevent Blindness, EyeSight Foundation of Alabama, Buck Trust of Alabama, and NIH P30 EY003039. A part of this work was presented at the ARVO 2013 annual meeting. Contributions of authors: conception and design (YZ, CO and CAC); analysis and interpretation (YZ, XW, and CAC); writing the manuscript (YZ); critical revision of the manuscript (YZ, CAG, RFS, CO, and CAC); final approval of the article (YZ, XW, EBR, MEC, CDW, RFS, CAG, CO, and CAC); data collection (YZ, XW, EBR, and MEC); obtaining funding (YZ, CAG, CO, and CAC); and literature search (YZ, RFS, and CAC); technical support and clinical supervision (CDW).

## References


1. Mimoun G, Soubrane G, Coscas G. Le drusen maculaires. J Fr Ophthalmol. 1990; 13(10):511–530.
2. Arnold JJ, Sarks SH, Killingsworth MC, Sarks JP. Reticular pseudodrusen. A risk factor in age-related maculopathy. Retina. 1995; 15(3):183–191. [PubMed: 7569344]
3. Lois N, Owens SL, Coco R, Hopkins J, Fitzke FW, Bird AC. Fundus autofluorescence in patients with age-related macular degeneration and high risk of visual loss. Am J Ophthalmol. 2002; 133(3): 341–349. [PubMed: 11860971]
4. Smith RT, Chan JK, Busuoic M, Sivagnanavel V, Bird AC, Chong NV. Autofluorescence characteristics of early, atrophic, and high-risk fellow eyes in age-related macular degeneration. Invest Ophthalmol Vis Sci. 2006; 47(12):5495–5504. [PubMed: 17122141]
5. Smith RT, Sohrab MA, Busuioc M, Barile G. Reticular macular disease. Am J Ophthalmol. 2009; 148(5):733–743. [PubMed: 19878758]
6. Zweifel SA, Spaide RF, Curcio CA, Malek G, Imamura Y. Reticular pseudodrusen are subretinal drusenoid deposits. Ophthalmology. 2010; 117(2):303–312. [PubMed: 19815280]
7. Rudolf M, Malek G, Messinger JD, Clark ME, Wang L, Curcio CA. Sub-retinal drusenoid deposits in human retina: organization and composition. Exp Eye Res. 2008; 87(5):402–408. [PubMed: 18721807]
8. Schmitz-Valckenberg S, Steinberg JS, Fleckenstein M, Visvalingam S, Brinkmann CK, Holz FG. Combined confocal scanning laser ophthalmoscopy and spectral-domain optical coherence tomography imaging of reticular drusen associated with age-related macular degeneration. Ophthalmology. 2010; 117(6):1169–1176. [PubMed: 20163861]
9. Querques G, Querques L, Martinelli D, et al. Pathologic insights from integrated imaging of reticular pseudodrusen in age-related macular degeneration. Retina. 2011; 31(3):518–526. [PubMed: 21150696]
10. Sohrab MA, Smith RT, Salehi-Had H, Sadda SR, Fawzi AA. Image registration and multimodal imaging of reticular pseudodrusen. Invest Ophthalmol Vis Sci. 2011; 52(8):5743–5748. [PubMed: 21693600]
11. Suzuki M, Sato T, Spaide RF. Pseudodrusen subtypes as delineated by multimodal imaging of the fundus. Am J Ophthalmol. 2014; 157(5):1005–1012. [PubMed: 24503406]
12. Sarks JP, Sarks SH, Killingsworth MC. Evolution of geographic atrophy of the retinal pigment epithelium. Eye. 1988; 2(Pt 5):552–577. [PubMed: 2476333]
13. Oak AS, Messinger JD, Curcio CA. Subretinal drusenoid deposits: further characterization by lipid histochemistry. Retina. 2014; 34(4):825–826. [PubMed: 24589874]
14. Curcio CA, Messinger JD, Sloan KR, McGwin G, Medeiros NE, Spaide RF. Subretinal drusenoid deposits in non-neovascular age-related macular degeneration: morphology, prevalence, topography, and biogenesis model. Retina. 2013; 33(2):265–276. [PubMed: 23266879]
15. Sarks J, Arnold J, Ho IV, Sarks S, Killingsworth M. Evolution of reticular pseudodrusen. Br J Ophthalmol. 2011; 95(7):979–985. [PubMed: 21109695]
16. Spaide RF, Koizumi H, Pozzoni MC. Enhanced depth imaging spectral-domain optical coherence tomography. Am J Ophthalmol. 2008; 146(4):496–500. [PubMed: 18639219]
17. Spaide RF, Curcio CA. Drusen characterization with multimodal imaging. Retina. 2010; 30(9): 1441–1454. [PubMed: 20924263]
18. Mrejen S, Sato T, Curcio CA, Spaide RF. Assessing the cone photoreceptor mosaic in eyes with pseudodrusen and soft Drusen in vivo using adaptive optics imaging. Ophthalmology. 2014; 121(2):545–551. [PubMed: 24183341]
19. Roorda A, Romero-Borja F, Donnelly W III, Queener H, Hebert T, Campbell M. Adaptive optics scanning laser ophthalmoscopy. Opt Express. 2002; 10(9):405–412. [PubMed: 19436374]
20. Zhang Y, Poonja S, Roorda A. MEMS-based adaptive optics scanning laser ophthalmoscopy. Opt Lett. 2006; 31(9):1268–1270. [PubMed: 16642081]
21. Burns SA, Tumbar R, Elsner AE, Ferguson D, Hammer DX. Large-field-of-view, modular, stabilized, adaptive-optics-based scanning laser ophthalmoscope. J Opt Soc Am A Opt Image Sci Vis. 2007; 24(5):1313–1326. [PubMed: 17429477]

22. Chen DC, Jones SM, Silva DA, Olivier SS. High-resolution adaptive optics scanning laser ophthalmoscope with dual deformable mirrors. J Opt Soc Am A Opt Image Sci Vis. 2007; 24(5): 1305–1312. [PubMed: 17429476]
23. Roorda A. Applications of adaptive optics scanning laser ophthalmoscopy. Optom Vis Sci. 2010; 87(4):260–268. [PubMed: 20160657]
24. Rossi EA, Chung M, Dubra A, Hunter JJ, Merigan WH, Williams DR. Imaging retinal mosaics in the living eye. Eye. 2011; 25(3):301–308. [PubMed: 21390064]
25. Cohen SY, Dubois L, Tadayoni R, Delahaye-Mazza C, Debibie C, Quentel G. Prevalence of reticular pseudodrusen in age-related macular degeneration with newly diagnosed choroidal neovascularisation. Br J Ophthalmol. 2007; 91(3):354–359. [PubMed: 16973663]
26. Schmitz-Valckenberg S, Alten F, Steinberg JS, et al. Reticular drusen associated with geographic atrophy in age-related macular degeneration. Invest Ophthalmol Vis Sci. 2011; 52(9):5009–5015. [PubMed: 21498612]
27. Lee MY, Yoon J, Ham DI. Clinical features of reticular pseudodrusen according to the fundus distribution. Br J Ophthalmol. 2012; 96(9):1222–1226. [PubMed: 22773089]
28. Querques G, Srour M, Massamba N, Puche N, Souied EH. Reticular pseudodrusen. Ophthalmology. 2013; 120(4):872–872. e874. [PubMed: 23552084]
29. Ueda-Arakawa N, Ooto S, Nakata I, et al. Prevalence and genomic association of reticular pseudodrusen in age-related macular degeneration. Am J Ophthalmol. 2013; 155(2):260–269. [PubMed: 23111182]
30. Ueda-Arakawa N, Ooto S, Tsujikawa A, Yamashiro K, Oishi A, Yoshimura N. Sensitivity and specificity of detecting reticular pseudodrusen in multimodal imaging in Japanese patients. Retina. 2013; 33(3):490–497. [PubMed: 23403515]
31. Ooto S, Ellabban AA, Ueda-Arakawa N, et al. Reduction of retinal sensitivity in eyes with reticular pseudodrusen. Am J Ophthalmol. 2013; 156(6):1184–1191. [PubMed: 23972310]
32. Lee MY, Ham DI. Subretinal drusenoid deposits with increased autofluorescence in eyes with reticular pseudodrusen. Retina. 2014; 34(1):69–76. [PubMed: 23743636]
33. Switzer DW, Engelbert M, Freund KB. Spectral domain optical coherence tomography macular cube scans and retinal pigment epithelium/drusen maps may fail to display subretinal drusenoid deposits (reticular pseudodrusen) in eyes with non-neovascular age-related macular degeneration. Eye. 2011; 25(10):1379–1380. [PubMed: 21738232]
34. Davis MD, Gangnon RE, Lee LY, et al. The Age-Related Eye Disease Study severity scale for age-related macular degeneration: AREDS Report No 17. Arch Ophthalmol. 2005; 123(11):1484–1498. [PubMed: 16286610]
35. Meadway A, Girkin CA, Zhang Y. A dual-modal retinal imaging system with adaptive optics. Opt Express. 2013; 21(24):29792–29807. [PubMed: 24514529]
36. Meadway A, Wang X, Curcio CA, Zhang Y. Microstructure of subretinal drusenoid deposits revealed by adaptive optics imaging. Biomed Opt Express. 2014; 5(3):713. [PubMed: 24688808]
37. Doble N, Miller DT, Yoon G, Williams DR. Requirements for discrete actuator and segmented wavefront correctors for aberration compensation in two large populations of human eyes. Appl Opt. 2007; 46(20):4501–4514. [PubMed: 17579706]
38. McLellan JS, Marcos S, Burns SA. Age-related changes in monochromatic wave aberrations of the human eye. Invest Ophthalmol Vis Sci. 2001; 42(6):1390–1395. [PubMed: 11328756]
39. Putnam NM, Hammer DX, Zhang Y, Merino D, Roorda A. Modeling the foveal cone mosaic imaged with adaptive optics scanning laser ophthalmoscopy. Opt Express. 2010; 18(24):24902–24916. [PubMed: 21164835]
40. Delori FC, Webb RH, Sliney DH. American National Standards I. Maximum permissible exposures for ocular safety (ANSI 2000), with emphasis on ophthalmic devices. J Opt Soc Am A Opt Image Sci Vis. 2007; 24(5):1250–1265. [PubMed: 17429471]
41. Beck RW, Moke PS, Turpin AH, et al. A computerized method of visual acuity testing: adaptation of the early treatment of diabetic retinopathy study testing protocol. Am J Ophthalmol. 2003; 135(2):194–205. [PubMed: 12566024]
42. Vogel CR, Arathorn DW, Roorda A, Parker A. Retinal motion estimation in adaptive optics scanning laser ophthalmoscopy. Opt Express. 2006; 14(2):487–497. [PubMed: 19503363]

43. Spaide RF, Curcio CA. Anatomical correlates to the bands seen in the outer retina by optical coherence tomography: literature review and model. Retina. 2011; 31(8):1609–1619. [PubMed: 21844839]
44. Spaide RF. Questioning optical coherence tomography. Ophthalmology. 2012; 119(11):2203–2204. [PubMed: 23122463]
45. Staurenghi G, Sadda S, Chakravarthy U, Spaide RF. Proposed lexicon for anatomic landmarks in normal posterior segment spectral-domain optical coherence tomography: the IN•OCT consensus. Ophthalmology. 201410.1016/j.ophtha.2014.02.023
46. Pallikaris A, Williams DR, Hofer H. The reflectance of single cones in the living human eye. Invest Ophthalmol Vis Sci. 2003; 44(10):4580–4592. [PubMed: 14507907]
47. Cooper RF, Dubis AM, Pavaskar A, Rha J, Dubra A, Carroll J. Spatial and temporal variation of rod photoreceptor reflectance in the human retina. Biomed Opt Express. 2011; 2(9):2577–2589. [PubMed: 21991550]
48. Wilson, T.; Sheppard, C. Theory and Practice of Scanning Optical Microscopy. London: Academic Press; 1984. p. 1-213.
49. Roorda A, Williams DR. Optical fiber properties of individual human cones. J Vis. 2002; 2(5):404–412. [PubMed: 12678654]
50. Enoch JM. Optical Properties of the Retinal Receptors. J Opt Soc Am A Opt Image Sci Vis. 1963; 53(1):71–85.
51. Stiles WS, Crawford BH. The Luminous Efficiency of Rays Entering the Eye Pupil at Different Points. Proc R Soc Lond B. 1933; 112(778):428–450.
52. Delint PJ, Berendschot TT, van Norren D. Local photoreceptor alignment measured with a scanning laser ophthalmoscope. Vision Res. 1997; 37(2):243–248. [PubMed: 9068824]
53. Di Francia GT, Ronchi L. Directional scattering of light by the human retina. J Opt Soc Am A Opt Image Sci Vis. 1952; 42(10):782–783.
54. Laties, AM.; Burnside, B. The maintenance of photoreceptor orientation. In: Pepe, FA.; Sanger, JW.; Nachmias, VT., editors. Motility and Cell Function: Proceedings of the First John M. Marshall Symposium in Cell Biology. New York: Academic Press; 1979. p. 285-298.
55. Laties AM, Enoch JM. An analysis of retinal receptor orientation I. Angular relationship of neighboring photoreceptors. Invest Ophthalmol Vis Sci. 1971; 10(1):69–77.
56. Burns SA, Wu S, Delori F, Elsner AE. Direct measurement of human-conephotoreceptor alignment. J Opt Soc Am A Opt Image Sci Vis. 1995; 12(10):2329–2338. [PubMed: 7500214]
57. Burns SA, Wu S, He JC, Elsner AE. Variations in photoreceptor directionality across the central retina. J Opt Soc Am A Opt Image Sci Vis. 1997; 14(9):2033–2040. [PubMed: 9291599]
58. Lujan BJ, Roorda A, Knighton RW, Carroll J. Revealing Henle's fiber layer using spectral domain optical coherence tomography. Invest Ophthalmol Vis Sci. 2011; 52(3):1486–1492. [PubMed: 21071737]
59. Alten F, Clemens CR, Heiduschka P, Eter N. Localized reticular pseudodrusen and their topographic relation to choroidal watershed zones and changes in choroidal volumes. Invest Ophthalmol Vis Sci. 2013; 54(5):3250–3257. [PubMed: 23599330]
60. Switzer DW Jr, Mendonca LS, Saito M, Zweifel SA, Spaide RF. Segregation of ophthalmoscopic characteristics according to choroidal thickness in patients with early age-related macular degeneration. Retina. 2012; 32(7):1265–1271. [PubMed: 22222760]
61. Querques G, Querques L, Forte R, Massamba N, Coscas F, Souied EH. Choroidal changes associated with reticular pseudodrusen. Invest Ophthalmol Vis Sci. 2012; 53(3):1258–1263. [PubMed: 22222508]
62. Haas P, Esmaeelpour M, Ansari-Shahrezaei S, Drexler W, Binder S. Choroidal thickness in patients with reticular pseudodrusen using 3D 1060-nm OCT maps. Invest Ophthalmol Vis Sci. 2014; 55(4):2674–2681. [PubMed: 24651554]
63. Sohrab M, Wu K, Fawzi AA. A pilot study of morphometric analysis of choroidal vasculature in Vivo using en face optical coherence tomography. PLoS ONE. 2012; 7(11):e48631. [PubMed: 23189132]
64. Ferris FL 3rd, Wilkinson CP, Bird A, et al. Clinical classification of age-related macular degeneration. Ophthalmology. 2013; 120(4):844–851. [PubMed: 23332590]

65. Mrejen S, Gallego-Pinazo R, Freund K, Paques M. Recognition of Henle's fiber layer on OCT images. Ophthalmology. 2013; 120(6):32–33.

66. Curcio CA, Messinger JD, Sloan KR, Mitra A, McGwin G, Spaide RF. Human chorioretinal layer thicknesses measured in macula-wide, high-resolution histologic sections. Invest Ophthalmol Vis Sci. 2011; 52(7):3943–3954. [PubMed: 21421869]

## Biography

Yuhua Zhang, PhD, is Assistant Professor of Ophthalmology at the Department of Ophthalmology, University of Alabama. His research interests are in adaptive optics scanning laser ophthalmoscopy and optical coherence tomography, and age-related macular degeneration. He leads the "Adaptive Optics Retinal Imaging Lab," which is funded by the EyeSight Foundation of Alabama, the International Retinal Research Foundation, and the National Eye Institute.

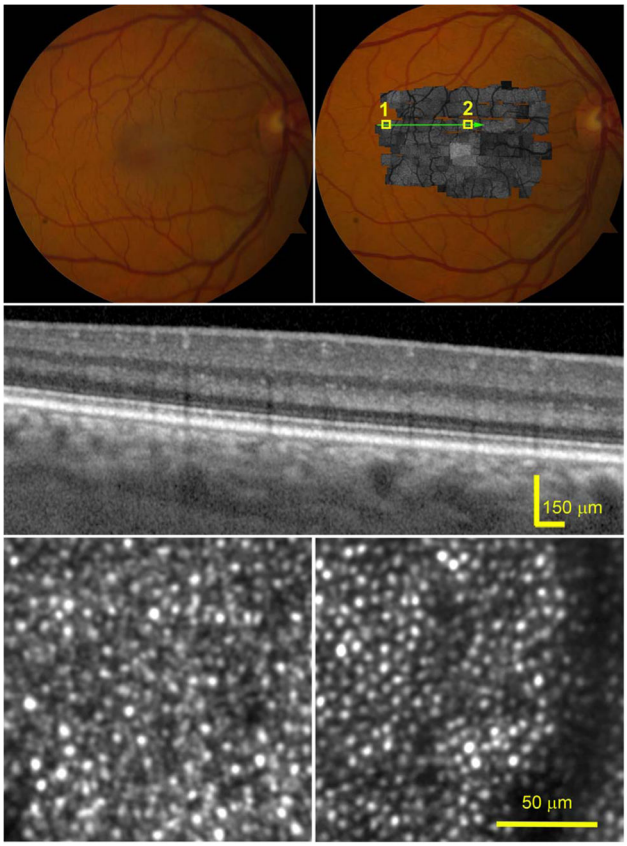


**Figure 1.**

Photoreceptors in a healthy retina imaged by adaptive optics scanning laser ophthalmoscopy (AOSLO) and spectral domain optical coherence tomography (SD-OCT) with enhanced depth imaging. The subject (AMD-051) is a 54-year-old man (Age-Related Eye Disease Study grade 1, best-corrected visual acuity 20/20). (Top row, left) Digital color fundus photograph of 30° field of vie w. (Top row, right) AOSLO montage in grayscale is overlaid on the fundus photograph. (Middle) SD-OCT B-Scans taken through the green arrow-line in the top-right panel show parallel and evenly reflective bands of the external limiting membrane (ELM), ellipsoidal zone (EZ), and the retinal pigment epithelium (RPE)-Bruch complex, with negligible diffuse accumulations between the EZ and RPE-Bruch complex. (Bottom row) AOSLO images contained in the boxes of the top-right panel, revealing clear photoreceptor mosaic. (Bottom row, left) Photoreceptors in the peripheral retina, box 1 in the top-right panel. Large, bright dots are cones, surrounded by smaller, dimmer dots representing rods. (Bottom row, right) Image was taken in the parafovea, box 2 in the top-right panel, most cells are cones. The dark band is the shadow of a retinal capillary. The reflectivity of individual photoreceptor varies,[46] but there is no significant change of areal reflectivity on the retina.

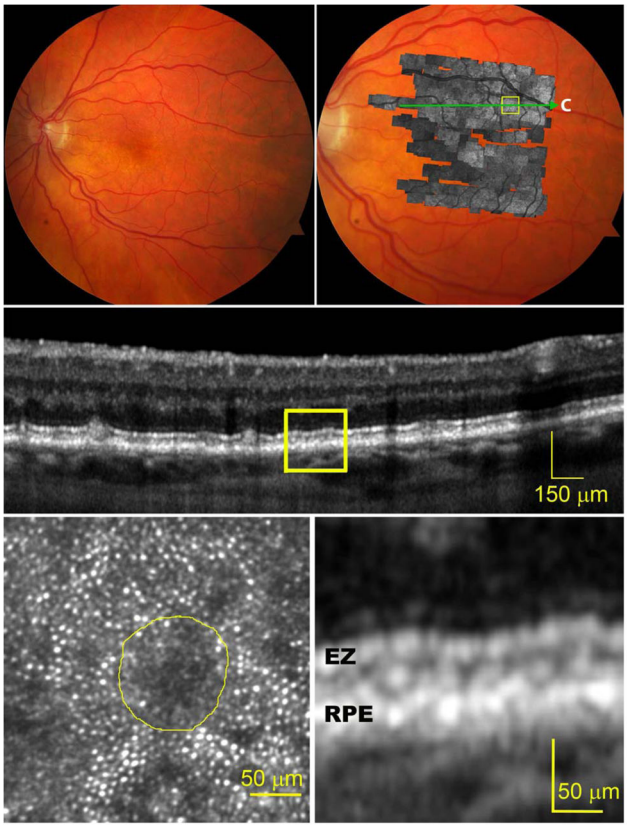


**Figure 2.**

Photoreceptors overlying a stage 1 subretinal drusenoid deposit imaged by adaptive optics scanning laser ophthalmoscopy (AOSLO) and spectral domain optical coherence tomography (SD-OCT) with enhanced depth imaging. The subject (AMD-058) is a 76-year-old woman with non-neovascular age-related macular degeneration (Age-Related Eye Disease Study grade 4, best-corrected visual acuity 20/25). (Top row, left) Digital color fundus photograph of 30° field of vie w. (Top row, right) AOSLO in gray scale is overlaid on the fundus photograph. (Middle) A SD-OCT B-Scan taken along the green arrow-line in top-right panel, showing undulating external limiting membrane (ELM) and ellipsoidal zone (EZ) bands. Diffuse deposition of granular hyper-reflective material between the retinal pigment epithelium (RPE) and the EZ is clearly observable at higher magnification in the bottom-right panel. (Bottom row, left) An AOSLO image of the area contained in box of the top-right panel reveals that photoreceptor mosaic overlaying a subretinal drusenoid deposit, delineated by the yellow boundary line, is undetectable and overall reflectivity is reduced.

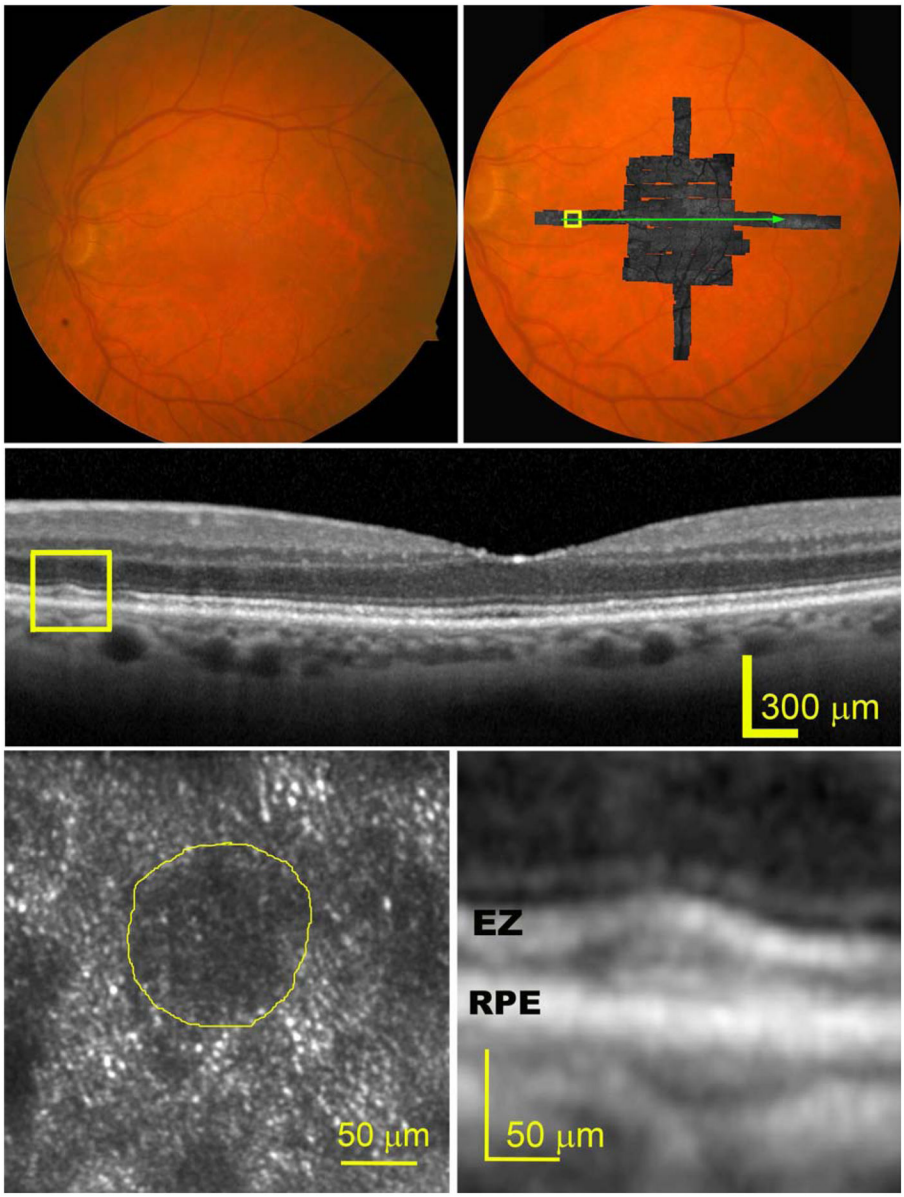


**Figure 3.**

Photoreceptors overlying a stage 2 subretinal drusenoid deposit imaged by adaptive optics scanning laser ophthalmoscopy (AOSLO) and spectral domain optical coherence tomography (SD-OCT) with enhanced depth imaging. The subject (AMD-041) is a 73-year-old man with non-neovascular AMD (Age-Related Eye Disease Study grade 6, best-corrected visual acuity 20/25). (Top row, left) Digital color fundus photograph of 30° field of view. (Top row, right) A OSLO montage in grayscale is overlaid on the fundus photograph. (Middle) A SD-OCT B-Scan taken along the green arrow-line in top-right panel shows that external limiting membrane (ELM) and ellipsoidal zone (EZ) bands are significantly altered by a large subretinal drusenoid deposit between the retinal pigment epithelium (RPE) and the EZ bands (magnified in the bottom-right panel). (Bottom row, left), An AOSLO image of the boxed region of panel A shows that photoreceptors overlying

the subretinal drusenoid deposit, delineated by the yellow boundary line, are invisible, and overall reflectivity is further reduced.

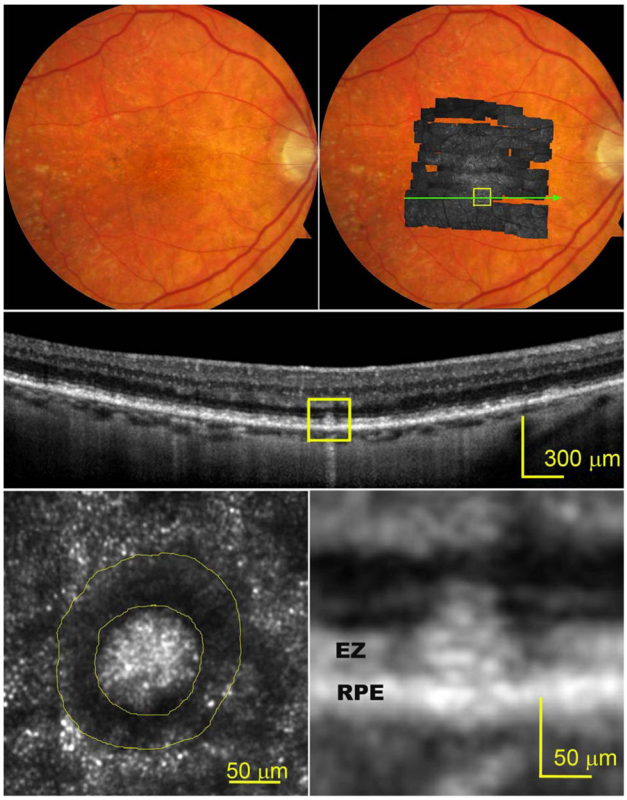


**Figure 4.**

A distinctive hyporeflective annulus with internal granular reflectivity typifies stage 3 subretinal drusenoid deposits imaged by adaptive optics scanning laser ophthalmoscopy (AOSLO) and spectral domain optical coherence tomography (SD-OCT) with enhanced depth imaging. The subject (AMD-63) is an 83-year-old man with non-neovascular age-related macular degeneration (Age-Related Eye Disease Study grade 7, best-corrected visual acuity 20/30). (Top row, left) Digital color fundus photograph of 30° field of view. (Top row, right) A OSLO montage in grayscale is overlaid on the fundus photograph. (Middle row) A SD-OCT B-Scan taken along the green arrow-line in the top-right panel shows that a large subretinal drusenoid deposit has interrupted the photoreceptor ellipsoidal zone (EZ) band and expanded into the external limiting membrane (ELM) band, shown at higher magnification in the bottom-right panel. (Bottom row, left) The AOSLO image of the contained in the box of the top-right panel reveals over the subretinal drusenoid deposit a hyporeflective ring surrounding a granular hyper-reflective center area. The hyporeflective ring corresponds to the ‘gap’ in the photoreceptor EZ on either side of the subretinal drusenoid deposits.

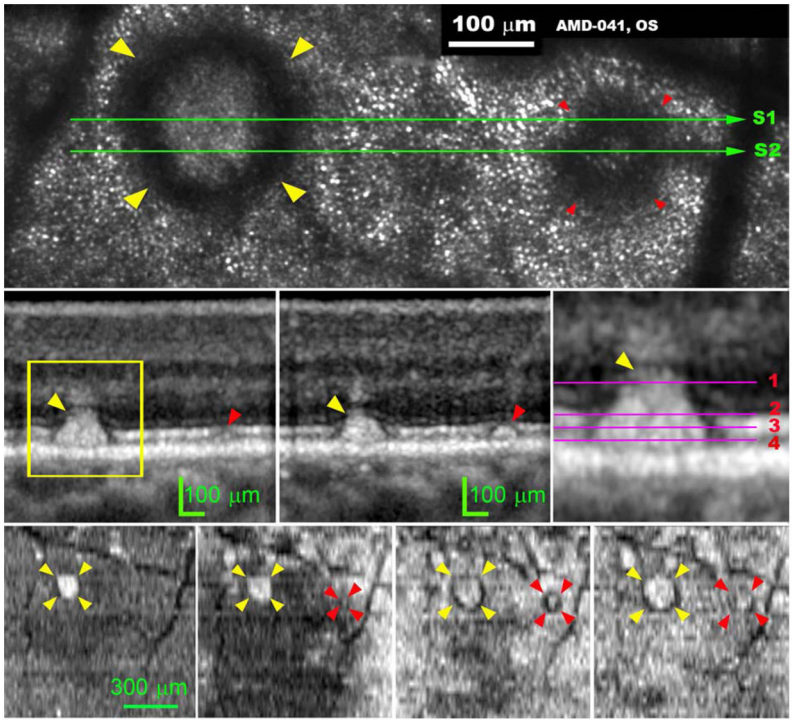


**Figure 5.**

Subretinal drusenoid deposit shape and location characterized by 3D and high-resolution imaging deposits imaged by adaptive optics scanning laser ophthalmoscopy (AOSLO) and spectral domain optical coherence tomography (SD-OCT). The subject (AMD-041) is a 73-year-old man with non-neovascular age-related macular degeneration (Age-Related Eye Disease Study grade 6, best-corrected visual acuity 20/25). (Top row) AOSLO image, cone photoreceptors are represented by evenly spaced hyper-reflective spots outside the annuli of hyper-reflectivity. The dark vertical bands are the shadows of overlying retinal blood vessels. The yellow and red arrowheads indicate a prominent stage 3 and stage 2 subretinal drusenoid deposits in superior perifovea, respectively, followed through the remaining panels. (Middle row, left and middle) OCT scans through these subretinal drusenoid deposits, as marked by the green line S1 and S2 in the top row panel. The stage 3 subretinal drusenoid deposit lifts the external limiting membrane (ELM) upward and is associated with a crowning tuft of hyper-reflectivity within the inner outer nuclear layer (ONL), representing perturbed Henle fibers.[58, 65, 66] The stage 2 subretinal drusenoid deposit indents but does not interrupt the photoreceptor ellipsoidal zone (EZ). (Middle row, right) Magenta lines mark the planes where *en-face* OCT images, shown in the bottom row panels from left to right, were extracted from the 3D volume OCT scan. AOSLO image was an integration of the light reflected from depth 1 through 4. (Bottom row, far left) The top of a stage 3 subretinal drusenoid deposits has reached the hypo-reflective band internal to ELM. The stage 3 subretinal drusenoid deposit manifests as a highly reflective area on the *en face* OCT image. (Bottom row, left) at the level near the EZ, the stage 3 subretinal drusenoid deposit becomes larger than at its apex. The stage 2 subretinal drusenoid deposit is barely eligible at this level. (Bottom row, right) at the middle of the EZ, the stage 3 subretinal drusenoid deposit is larger still, and a dark annulus appears; so does the stage 2 subretinal drusenoid deposit.

(Bottom row, far right) Near the retinal pigment epithelium (RPE), the hyper-reflective center and hyporeflective annulus of the stage 3 subretinal drusenoid deposit are at their largest. However, the stage 2 subretinal drusenoid deposit is indistinct at this level. The stage 3 subretinal drusenoid deposit shows a wide hyporeflective ring with indistinct borders. The ‘gap’ in the EZ on either side of subretinal drusenoid deposits in the OCT B-scan corresponds to the hyporeflective annulus on the en-face OCT and the AOSLO image.

## TABLE

Subretinal drusenoid deposits and subretinal drusenoid deposits-associated impact on photoreceptors

| Size | Stage 1 | Stage 2 | Stage 3 | |
|---|---|---|---|---|
| | | | Inner diameter [b] | Outer diameter [c] |
| Mean ± SD (μm)[a] | 78.02 ± 23.60 | 92.55 ± 26.06 | 59.51 ± 19.87 | 123.30 ± 29.70 |
| Range (μm) | 43.37 – 159.56 | 43.37 – 169.07 | 25.89 – 131.16 | 66.03 – 235.85 |

[a] SD: standard deviation.

[b] The diameters of the reflective cores of stage 3 subretinal drusenoid deposits.

[c] The diameters of the hyporeflective annuli of stage 3 subretinal drusenoid deposits.